J|A|C|S ARTICLES

Published on Web 03/20/2009

A Mixed-Valence V^{IV}/V^{V} Alkoxo-polyoxovanadium Cluster Series $[V_6O_8(OCH_3)_{11}]^{n+/-}$: Exploring the Influence of a μ-Oxo Ligand in a Spin Frustrated Structure

Charles Daniel* and Hans Hartl

Institute of Chemistry and Biochemistry/Inorganic Chemistry, Freie Universität Berlin, Fabeckstrasse 34-36, 14195 Berlin, Germany

Received September 17, 2008; E-mail: charles.daniel@web.de

Abstract: The synthesis and structural characterization of the neutral mixed-valence methoxo-polyoxovanadium cluster $[V_6O_8(OCH_3)_{11}]$ (**1**) and its single oxidation product in the hexachloroantimonate salt $[V_6O_8(OCH_3)_{11}][SbCl_6]$ (**2**) are presented here. The cluster comprises a hexauclear polyoxovanadate core of the Lindqvist structure, of which all but one of the μ-bridging oxo ligands are substituted by methoxo. As revealed by cyclic voltammetry, the cluster is highly redox active, displaying several further thermodynamically stable V^{IV}/V^{V} mixed-valence redox derivatives. Furthermore, valence sum calculations performed on the X-ray structural data as well as results from IR and UV−vis spectrometry characterize them as class II mixed-valence compounds. In the present article, we equally present results from cyclic voltammetry, UV−vis spectrometry, and magnetic measurements obtained for members of the previously reported $[V_6O_7(OCH_3)_{12}]$ cluster series, which, as opposed to **1** and its derivatives, contain exclusively methoxo ligands as μ-bridging moieties. Magnetic measurements performed on the highly reduced cluster species $[V^{IV}_5V^{V}_1O_7(OCH_3)_{12}]^{-}$ and $[V^{IV}_6O_7(OCH_3)_{12}]^{2-}$ reveal net antiferromagnetic exchange interactions between the d-electrons, which at lower temperatures are in part suppressed for reasons attributed to geometric spin frustration. Among the present results, the comparison of the cyclic voltammograms of **1** and $[V_6O_7(OCH_3)_{12}]$ has proven to be of considerable interest, showing an unexpectedly pronounced discrepancy in all but one of their corresponding redox potentials. In particular, a detailed analysis of the electrochemical conversions indicates that the observed shift is almost entirely the result of a different degree of d-electron spin−spin interactions in corresponding mixed valence species of the cluster series.

Introduction

Polyoxometalates constitute a large class of discrete metal-oxide entities displaying a wide variety of structures.[1,2] These compounds are of particular interest since they combine concepts of classical solid state chemistry with molecular chemistry, thus extending metal-oxide chemistry to the molecular level. As a result of their unique features, they are not only the object of intense and ongoing research but have also found a wide application in various domains including the field of medicine and material science,[3] not to mention their importance in catalysis.[4]

The classical polyoxometalates have been greatly furthered by the introduction of organic ligands into polyoxometalate synthesis, giving access to a shear wealth of new polyoxometalate architectures.[5] This methodology also permitted the synthesis of compounds comprising the hexavanadate core $\{V_6O_{19}\}$,[6] a classical polyoxometalate structure that until then was only known for Mo, W, Nb and Ta. In particular, Zubieta et al. were successful in synthesizing a variety of these hexavanadate derivatives with the help of trisalkoxo μ-bridging moieties,[7] revealing a rich class of V^{IV}/V^{V} mixed valence compounds with highly interesting electronic and magnetic properties.[8−10]

We have previously reported on novel alkoxo-polyoxovanadium cluster[11] compounds of the general composition $[V_6O_7(OR)_{12}]$ (R = $-CH_3$, $-C_2H_5$).[9,10] These clusters are formally derived from the highly symmetrical Lindqvist structure[12] $[M_6O_{19}]^{n-}$ (Figure 1) through substitution of all 12 μ-bridging

(1) Pope, M. T. *Heteropoly and Isopoly Oxometalates*; Springer: Berlin, 1983.
(2) (a) Baker, L. C.; Glick, D. C. *Chem. Rev.* **1998**, *1*, 3–49. (b) Pope, M. T. In *Comprehensive Coordination Chemistry II*; McCleverty, J. A., Meyer, T. J., Eds.; Elsevier: Oxford 2004; Vol. 4, pp 635−678.
(3) (a) Pope, M. T.; Müller, A. *Angew. Chem., Int. Ed. Engl.* **1991**, *30*, 34–48. (b) *Polyoxometalates: From Platonic Solids to Anti-Retroviral Activity*; Pope, M. T., Müller, A., Eds.; Kluwer: Dordrecht, 1994. (c) Polyoxometalates. In *Chemical Reviews*; Hill, C., Ed; American Chemical Society: Washington, DC, 1988. (d) *Polyoxometalate Chemistry: From Topology via Self-Assembly to Applications*; Pope, M. T., Müller, A., Eds.; Kluwer: Dordrecht, 2001. (e) *Polyoxometalate Chemistry for Nano-Composite Design*; Yamase, T., Pope, M. T., Eds.; Kluwer/Plenum: New York, 2002. (f) *Polyoxometalate Molecular Science*; Borrás-Almenar, J. J., Coronado, E., Müller, A., Pope, M. T., Eds.; Kluwer: Dordrecht, 2003.
(4) (a) Kozevnikov, I. *Catalysis by Polyoxometalates*; John Wiley & Sons: Chichester, 2002. (b) Hill, C. L. In *Comprehensive Coordination Chemistry II*; McCleverty, J. A., Meyer, T. J., Eds.; Elsevier: Oxford 2004; Vol. 4, pp 679−759.
(5) Gouzerh, P.; Proust, A. *Chem. Rev.* **1998**, *98*, 77–111.
(6) see also (a) Hayashi, Y.; Ozawa, Y.; Isobe, K. *Chem. Lett.* **1989**, 425. (b) Chae, H. K.; Klemperer, W. G.; Day, V. W. *Inorg. Chem.* **1989**, *28*, 1423. (c) Hayashi, Y.; Ozawa, Y.; Isobe, K. *Inorg. Chem.* **1991**, *30*, 1025–1033.
(7) Khan, M. I.; Zubieta, J. *Prog. Inorg. Chem.* **1995**, *43*, 1–149.

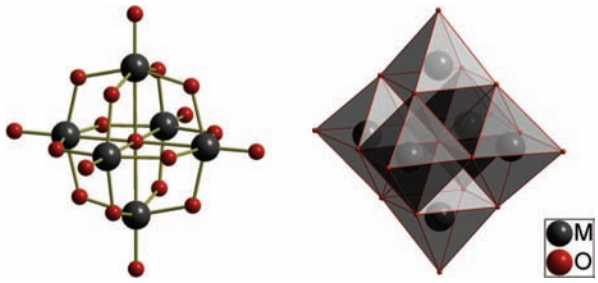

Figure 1. Lindqvist structure: ball and stick and coordination polyhedron models.

oxo ligands by monodentate alkoxo ligands. Certainly the most outstanding feature of these clusters lies in their high redox activity, cyclic voltammetry revealing a series of thermodynamically stable redox isomers $[V^{IV}_{n}V^{V}_{6-n}O_7(OR)_{12}]^{(4-n)}$, of which numerous species have been chemically synthesized and characterized (R = -CH_3, $n = 3-6$; R = -C_2H_5, $n = 2-4$).[9,10,13]

In addition to this, investigation of intervalence charge transfer (IVCT) in the V^{IV}/V^{V} mixed valence species based on results obtained from IR spectroscopy, cyclic voltammetry, and valence sum calculations conducted on the basis of the crystal structure analysis has revealed that they are well-behaved class II mixed valence compounds according to the Robin and Day classification scheme.[14] The d-electron of the vanadium(+IV) nuclei can therefore be extensively delocalized in the highly symmetrical $\{V_6O_{19}\}$ hexavanadate core.[10] Elaborate EPR studies conducted on the neutral cluster species indicates that electron transfer phenomena even persist when cooling down to liquid helium temperatures.[15]

The neutral $[V_6O_7(OCH_3)_{12}]$ cluster has also been the object of extensive mass spectrometric studies using electrospray ionization[16] and is presently an invaluable precursor for the generation of numerous charged vanadium-oxide clusters in the gas phase,[17] of which the cationic species prove highly reactive in ion−molecule reactions.[18] In addition to this, quantum-chemical calculations have been conducted on this cluster species within the DFT framework.[19]

In the present article, we have extended our investigation of the $[V_6O_7(OCH_3)_{12}]^{n\pm}$ cluster series to include results from magnetic measurements and UV−vis spectroscopy, as well as from new cyclovoltammetric experiments which has furthered our insight into their redox behavior.

In addition to this, we presently report on a new cluster series, of which the μ_6-oxo-dodeca-μ-methoxo-hexakis(oxovanadium) cluster $[V_6O_8(OCH_3)_{11}]$ (**1**) constitutes the neutral species. This methoxo-polyoxovanadium compound has nearly the same chemical structure as the $[V_6O_7(OCH_3)_{12}]$ cluster, with the exception of one μ-bridging position which is occupied by an oxo ligand. Results from cyclic voltammetry show that **1** is also highly redox active, revealing a number of thermodynamically stable redox isomers of which the chemical synthesis and X-ray structural characterization of the single oxidation step product $[V_6O_8(OCH_3)_{11}][SbCl_6]$ (**2**) is presented here. Furthermore, IR and UV−vis spectroscopy as well as valence sum calculations performed on the X-ray structural data serve as a basis for the investigation of the mixed valence state in this new cluster series.

The main focus of the present article, however, concerns the exceptional quality of these cluster series as model compounds for the investigation of spin−spin interactions between unpaired d-electrons in cluster entities comprising transition metal centers linked by superexchange mediating ligands. As will be shown from the cyclovoltammetric results, the present clusters can be completely oxidized to species devoid of d-electrons and then subsequently reduced in discrete single-electron reduction steps to mixed valence species with one and two delocalized d-electrons, in a well-behaved electrochemical process. Accordingly, it is presently possible to assess the transition from valence states devoid of interelectronic interactions, to those in which spin−spin interactions are first made possible.

In this respect, different magnitudes of superexchange interactions due to the formal exchange of a single μ-bridging methoxo ligand in the $[V_6O_7(OCH_3)_{12}]^{n\pm}$ series for a μ-bridging oxo ligand in the $[V_6O_8(OCH_3)_{11}]^{n\pm}$ series leads to a surprisingly strong discrepancy in their respective redox properties. In fact, this constitutes, to our knowledge, the first example for the assessment of an electrochemical potential shift in a polynuclear metal-oxo cluster which may be directly attributed to a difference in spin−spin interactions between unpaired d-electrons.

On the basis of these observations, we consider that the present results may constitute substantial evidence for a particularly strong influence of superexchange interactions on the redox properties of cluster compounds comprising transition metal centers linked by superexchange mediating ligands. Considering the function of transition metal-oxo and -thio

(8) (a) Chen, Q.; Zubieta, J. *Inorg. Chem.* **1990**, *29*, 1458–1459. (b) Khan, M. I.; Chen, Q.; Zubieta, J.; Goshorn, D. P. *Inorg. Chem.* **1992**, *31*, 1556–1558. (c) Chen, Q.; Goshorn, D. P.; Scholes, C. P.; Tan, X.; Zubieta, J. *J. Am. Chem. Soc.* **1992**, *114*, 4667–4681. (d) Khan, M. I.; Chen, Q.; Höpe, H.; Parkin, S.; O'Connor, C. J.; Zubieta, J. *Inorg. Chem.* **1993**, *32*, 2929–2937. (e) Hou, D.; Kim, G.-S.; Hagen, K. S.; Hill, K. L. *Inorg. Chim. Acta* **1993**, *211*, 127–130. (f) Müller, A.; Meyer, J.; Bögge, H.; Stammler, A.; Botar, A. *Z. Anorg. Allg. Chem.* **1995**, *621*, 1818–1831. (g) Piepenbrink, M.; Triller, M. U.; Gorman, N. H. J.; Krebs, B. *Angew. Chem., Int. Ed.* **2002**, *41*, 2523–2525.
(9) Spandl, J.; Daniel, C.; Brüdgam, I.; Hartl, H. *Angew. Chem., Int. Ed.* **2003**, *42*, 1163–1166.
(10) Daniel, C.; Hartl, H. *J. Am. Chem. Soc.* **2005**, *127*, 13978–13987.
(11) The use of the term "cluster" for polyoxometalates is a topic of controversy. In our opinion, its use is legitimate since by definition a cluster compound's "*essential feature is a system of bonds connecting each atom directly to its neighbors in the polyhedron*", of which the "*atoms making up a cage or cluster may be different*" (cited from: Cotton, F. A.; Wilkinson, G.; Murillo, C. A.; Bochmann, M. *Advanced Inorganic Chemistry*; John Wiley & Sons: New York 1999). Polyoxometalates fulfil these requirements and may therefore correctly be regarded as metal-oxygen clusters.[3a] Furthermore, the commonly used terms[5] "alkoxo-polyoxometalate" or "polyoxoalkoxometalate" are unsuited for the compounds presented here as a whole, since the majority are either neutral or cationic.
(12) Lindqvist, I. *Ark. Kemi* **1953**, *5*, 247–250.
(13) Kessler, V. G.; Seisenbaeva, G. A. *Inorg. Chem. Commun.* **2000**, *3*, 203–204.
(14) Robin, M. P.; Day, P. *Adv. Inorg. Chem. Radiochem.* **1967**, *10*, 247–422.
(15) (a) Augustyniak-Jabłokow, M. A.; Borshch, S. A.; Daniel, C.; Hartl, H.; Yablokov, Y. V. *New J. Chem.* **2005**, *29*, 1–8. (b) Augustyniak-Jabłokow, M. A.; Daniel, C.; Hartl, H.; Spandl, J.; Yablokov, Y. V. *Inorg. Chem.* **2008**, *47*, 322–332.
(16) Schröder, D.; Engeser, M.; Brönstrup, M.; Daniel, C.; Spandl, J.; Hartl, H. *Int. J. Mass Spectrom.* **2003**, *228*, 743–757.
(17) Feyel, S.; Schwarz, H.; Schröder, D.; Daniel, C.; Hartl, H.; Döbler, J.; Sauer, J.; Santambrogio, G.; Wöste, L.; Asmis, K. *Chem. Phys. Chem.* **2007**, *8*, 1640–1647.
(18) (a) Feyel, S.; Schröder, D.; Rosanzka, X.; Sauer, J.; Schwarz, H. *Angew. Chem., Int. Ed.* **2006**, *45*, 4677–4681. (b) Feyel, S.; Döbler, J.; Schröder, D.; Sauer, J.; Schwarz, H. *Angew. Chem., Int. Ed.* **2006**, *45*, 4681–4685. (c) Feyel, S.; Scharfenberg, L.; Daniel, C.; Hartl, H.; Schröder, D.; Schwarz, H. *J. Phys. Chem. A* **2007**, *111*, 3278–3286.
(19) Zueva, E. M.; Borshch, S. A.; Petrova, M. M.; Chermette, H.; Kuznetsov, A. M. *Eur. J. Inorg. Chem.* **2007**, *431*, 7–4325.

clusters as redox centers in ubiquitous metalloproteins which master complex chemical transformations in nature, the present findings suggest that their versatility may very well rely on a pronounced sensitivity of their redox potentials toward structural and/or chemical modifications influencing the magnetic exchange interactions at work between their unpaired d-electrons.

Experimental Section

Reagent grade chemicals were used in all reactions. $VO(O^tBu)_3$ and $VO(OCH_3)_3$ were prepared according to literature procedure.[20,21]

In reactions involving Cl_2 and $SbCl_5$, Schlenk techniques were used throughout the procedure. Dichloromethane used as a solvent was thoroughly dried with CaH_2 and stored over molecular sieve (0.3 nm) prior to use. Chlorine was condensed under reduced pressure (~100 mbar) into a graduated capillary held at liquid nitrogen temperature, and thawed at −78 °C before further transfer by condensation into the reaction vessel. In all steps, care was taken to thoroughly dry the apparatus prior to use.

Reactions under solvothermal conditions were conducted in pressure digestion vessels (Berghof, DAB 2) containing 50 mL Teflon inserts. The water sensitive oxovanadium(V) alkoxides used in the reactions were weighed into the inserts in a glovebox, and the solvent and eventually further chemicals were added rapidly after removal from the glovebox's inert atmosphere before enclosure in the pressure digestion vessels.

Column chromatography was performed on 63−200 mesh silica gel (Merck). Silica gel 60 TLC aluminum sheets (Merck) were used for thin layer chromatography.

Solutions from extraction procedures containing reaction products were generally filtered clear through a syringe filter (Roth, Rotilabo, PTFE, 0.2 μm) prior to crystallization.

Preparation of $VO(OCH_3)_3$. All steps were carried out under inert conditions using Schlenk techniques. Forty-three grams (150 mmol) of $VO(O^tBu)_3$ were weighed into a 500 mL Schlenk flask and 250 mL dry methanol were added under vigorous stirring. After complete dissolution, the product rapidly crystallizes out of the solution. The pale-yellow precipitate was collected on a fritted Schlenk funnel and vaccuum-dried overnight (yield: 93%). ^{51}V-NMR (105.03 MHz; $CDCl_3$): δ [ppm] = −527 (s, 1V).

Preparation of $[V_6O_8(OCH_3)_{11}]$ (1). Two procedures were developed for the synthesis of **1**. The first method (A) provides higher yields but is more time-consuming than the second method (B).

Method A. Eight-tenths of a gram (5 mmol) of $VO(O^tBu)_3$, and 25 mL methanol were respectively placed in six 50 mL Teflon autoclave inserts, which were then each sealed in a pressure digestion vessel and heated 24 h at 125 °C. The resulting dark-green solutions were united and evaporated to dryness. The residue was then taken up in very little dichloromethane and chromatographed by column chromatography with hexane/acetone (2:1 by volume) on 63−200 mesh silica gel (Merck). The first green fraction (R_f 0.46) contains $[V_6O_7(OCH_3)_{12}]$, followed by a dark green fraction (R_f 0.41) containing the desired product. The second fraction was evaporated to dryness, and the black residue was repeatedly extracted with hexane until the extracting solution remained nearly colorless. The united solutions were then concentrated under reduced pressure and stored at −30 °C, yielding black, octahedral crystals of **1** (yield: 31%). Elemental analysis calcd (%) for $C_{11}H_{33}O_{19}V_6$ (M = 775.02 g/mol): C 17.05, H 4.29; found: C 17.02, H 4.19. IR (KBr pellet, cm^{-1}): 1169 (w), 1143 (w), 1025 (vs), 975 (vs), 715 (m), 588 (s), 435 (s), 411 (s).

Method B. Eight-tenths of a gram (5 mmol) of $VO(OCH_3)_3$ were respectively placed in six 50 mL Teflon autoclave inserts. To each were added 25 mL dry methanol and 2.1 mL of 0.8 M tetrabutylammonium hydroxide solution in methanol. The inserts were then sealed shut in pressure digestion vessels and heated for 24 h at 125 °C. The resulting green solutions were united in a 250 mL flask, to which a solution of 0.5 g (3.94 mmol) of iodine in 10 mL of methanol was added in 1 mL portions. After each addition, the solution was stirred for 5 min and the composition of the solution was then checked by thin layer chromatography (eluent: hexane/acetone 2:1 by volume), the product appearing as a dark green spot (R_f 0.41). The procedure was repeated until an orange spot appeared below the product on the TLC. The solution was then placed in a large separating funnel and extracted with 12 × 200 mL hexane. The extracting solutions were then united and evaporated to dryness. The black residue was then repeatedly extracted with hexane until the extracting solution remained nearly colorless. The united solutions were then concentrated under reduced pressure and stored at −30 °C, yielding black, octahedral crystals of **1** (yield: 9%). Elemental analysis calcd (%) for $C_{11}H_{33}O_{19}V_6$ (M = 775.02 g/mol): C 17.05, H 4.29; found: C 16.99, H 4.25.

Preparation of $[V_6O_8(OCH_3)_{11}][SbCl_6]$ (2). Two-hundred fifty-four milligrams (0.328 mmol)of **1** and 42 μL (0.331 mmol) of $SbCl_5$ were given into a 25 mL Schlenk tube. Fifteen milliliters of anhydrous dichloromethane and 25 μL (0.197 mmol) of Cl_2 were then successively condensed under reduced pressure into the Schlenk tube held at liquid nitrogen temperature. The reaction mixture was then thawed at −78 °C in an ethanol/dry ice bath and slowly let warm to RT while stirring overnight. The reaction solution was then evacuated to dryness and the residue extracted with 2 × 20 mL anhydrous dichloromethane. The solution was slightly concentrated under reduced pressure and stored at −30 °C yielding black, rod-shaped crystals of **2** · CH_2Cl_2 (yield: 89%). Elemental analysis calcd (%) for $C_{11}H_{33}O_{19}Cl_6V_6Sb$ (M = 1109.49 g/mol): C 11.91, H 3.00; found: C 11.87, H 2.92. IR (KBr pellet, cm^{-1}): 1170 (w), 1139 (vw), 1005 (vs), 990 (vs), 712 (m), 606 (m), 479 (vw), 438 (sh), 422 (m).

X-Ray Structure Analysis. Single-crystal diffractometry was conducted on a Bruker XPS diffractometer (CCD area detector, Mo Kα radiation, λ = 0.71073 Å, graphite monochromator). Empirical absorption correction was applied on the data using symmetry-equivalent reflections (SADABS). The structures were solved using direct methods[22] and refined based on F^2 data with a least-squares procedure[23] using the WinGX program system.[24] Anisotropic displacement parameters were assigned to all non-H atoms. The hydrogen atoms were calculated in geometrically idealized positions. Crystallographic data for compounds **1** and **2** at 173 K is summarized in Table 1.

For measurement, single crystals of the respective substances were taken directly out of the mother liquor and prepared under a liquid nitrogen cooled nitrogen gas stream.

Cyclic Voltammetry. Cyclovoltammetric investigations were carried out using a PCI4 potentiostat/galvanostat/ZRA from Gamry Instruments, Inc., using the software Framework (version 4.31). The data was processed with Echem Analyst (version 1.31). Figures containing cyclic voltammograms were produced with Microcal Origin (version 5.0).

Measurements were conducted in a custom-made graduated Schlenk cell with a capacity of 2−8 mL. The working concentration was approximately 10^{-3} mol·l^{-1} in anhydrous acetonitrile, using tetrabutylammonium hexafluorophosphate as the supporting electrolyte (0.1 M). Platinum wire electrodes were used as the working-, counter-, and quasi-reference electrode.

Measurements were performed as double-cycle experiments, beginning and ending at the open circuit potential $E' = 0$ V. Scan rates of 50, 100 and 200 mV·s^{-1} were used in the experiments. As

(20) Prandtl, W.; Hess, L. *Z. Anorg. Chem.* **1913**, *82*, 103–129.
(21) Spandl, J. *Doctoral Thesis*, Freie Universität, Berlin, Germany, 2001.
(22) (a) *SHELXS-97 - A program for automatic solution of crystal structures*; Sheldrick, G. M., Ed.; University of Göttingen: Germany, 1997; Release 97−2. (b) Altomare, A.; Gascarano, G.; Giacovazzo, C.; Gualardi, A. *J. Appl. Crystallogr.* **1993**, *26*, 343–350.
(23) *SHELXL-97 - A program for crystal structure refinement*; Sheldrick, G. M., Ed.; University of Göttingen: Germany, 1997; Release 97−2.
(24) Farrugia, L. J. *J. Appl. Crystallogr.* **1999**, *32*, 837–838.

Table 1. X-Ray Crystallographic Data for Compounds **1** and **2**

compound	**1**	**2** · CH_2Cl_2
formula	$C_{11}H_{33}O_{19}V_6$	$C_{12}H_{35}O_{19}Cl_8V_6Sb$
formula weight	775.02	1194.43
meas. temp. (K)	173	173
crystal morph.	octahedron	rod-shaped
crystal size (mm)	0.43 × 0.29 × 0.26	0.33 × 0.06 × 0.04
crystal system	monoclinic	triclinic
space group	$P2_1/n$	$P\bar{1}$
cell dimensions		
a (Å)	10.116(2)	10.074(2)
b (Å)	13.004(3)	13.066(3)
c (Å)	10.385(2)	15.085(3)
α	90.00°	90.041(5)°
β	97.720(4)°	103.880(5)°
γ	90.00°	91.872(5)°
cell volume (Å^3)	1353.8(4)	1926.5(7)
formula units Z	2	2
ρ_{calc} (g/cm^{-1})	1.901	2.059
μ (Mo Kα) (mm^{-1})	2.063	2.701
abs.corr., T_{min}/T_{max}	0.46/0.52	0.25/0.43
$\theta_{min}/\theta_{max}$ (deg)	2.52/30.53	1.39/25.08
coll. reflections	27410	16279
unique reflections	4137	6777
ls parameters	216	428
R_1 [$I > 2\sigma(I)$]	0.0319	0.0543
wR_2 [$I > 2\sigma(I)$]	0.0821	0.1314
R_1 (all data)	0.0386	0.0884
wR_2 (all data)	0.0889	0.1455
GoF	0.900	0.958
larg. diff. ± (e·Å^{-3})	1.15/−0.81	0.78/−1.59

recommended by IUPAC, the potentials $E^{0\prime}$ obtained in nonaqueous media are given versus the ferrocene/ferrocenium (Fc/Fc^+) couple (vs Fc).[25]

The cell preparation was carried out under inert conditions using Schlenk techniques. After adding the supporting electrolyte, the cell was thoroughly heated under reduced pressure. The cell was then allowed to cool, and the compound sample was added while simultaneously flushing with argon. Subsequently, 2 mL anhydrous solvent were condensed into the vessel. Finally, the cell was gently shaken to complete the dissolution of the substance and the supporting electrolyte before starting the measurement.

Magnetochemistry. Magnetic experiments were conducted on a SQUID magnetometer at the Max-Planck Institute of Solid State Research in Stuttgart. The measurements were performed in single scan-cycles in the 2−300 K temperature range at field strengths of 1, 3, and 5 T.

IR Spectroscopy. IR spectra were collected in the 400−4000 cm^{-1} region on a Nicolet 5 SXC FTIR spectrometer. The data was processed using the OMNIC E.S.P software (version 4.1 b). Figures containing IR spectra were produced with Microcal Origin (version 5.0).

UV−Vis Spectroscopy. UV−vis spectra were collected in the 200−1000 nm region using a single beam spectrometer Specord 40 (Analytik Jena). Figures containing UV−vis spectra were produced with Microcal Origin (version 5.0).

Results and Discussion

For ease of reading, we will refer to clusters belonging to the $[V_6O_8(OCH_3)_{11}]^{n\pm}$ series as *undeca*methoxo-clusters by virtue of containing eleven μ-bridging methoxo ligands. Consequently, cluster compounds belonging to the $[V_6O_7(OCH_3)_{12}]^{n\pm}$ cluster series well be referred to as *dodeca*methoxo-clusters.

Synthesis. As for the *dodeca*methoxo- and -ethoxo-clusters $[V_6O_7(OCH_3)_{12}]$ and $[V_6O_7(OC_2H_5)_{12}]$,[9,10] the *undeca*methoxo-cluster $[V_6O_8(OCH_3)_{11}]$ (**1**) presented here is obtained by solvothermal synthesis. In the following we will discuss alternative methods of synthesis for obtaining this neutral cluster compound.

The first method of synthesis (Method A) involves the solvothermal reaction $VO(O^tBu)_3$ and methanol previously thought to exclusively afford the *dodeca*methoxo-cluster $[V_6O_7(OCH_3)_{12}]$.[9] The procedure yields an apparently uniform, black crystalline product, which in reality is a mixture of crystals of $[V_6O_7(OCH_3)_{12}]$ and **1**. The highly similar characteristics of the crystalline compounds and the unexpected challenges in the X-ray structural elucidation of **1** (*vide infra*), however, led us to initially believe that the *dodeca*methoxo-cluster $[V_6O_7(OCH_3)_{12}]$ was in fact the sole product of this reaction.

In view of these findings, Method A consists in first obtaining a mixture of $[V_6O_7(OCH_3)_{12}]$ and $[V_6O_8(OCH_3)_{11}]$ (**1**) following this procedure and subsequently separating the compounds by column chromatography. Besides having the disadvantage of generating large amounts of *dodeca*methoxo-cluster, this procedure has the further drawback of requiring a tedious chromatographic purification step, since the compounds are highly similar in both their solubilities as well as in their absorption behavior toward chromatographic material. Thus, the R_f values for **1** and $[V_6O_7(OCH_3)_{12}]$ in hexane/acetone (2:1 by volume) on silica gel are of the order of 0.41 and 0.46 respectively, rendering their separation a time-consuming enterprise, especially when working on a larger scale.

For this reason, an alternative method of synthesis was explored in an attempt to selectively yield compound **1**. Such a procedure (Method B) has recently been discovered, involving the solvothermal reaction of $VO(OCH_3)_3$ with tetrabutylammonium hydroxide in methanol at 125 °C for 24 h. The resulting dark green solution is then treated with iodine, yielding $[V_6O_8(OCH_3)_{11}]$ (**1**). Evaporating the resulting solution to dryness at this stage, however, leads to the formation of byproduct which make subsequent chromatography necessary. For this reason, the product is directly extracted from the reaction solution with hexane. Although this approach selectively affords **1**, the yield is only modest (∼10%). Nevertheless, this procedure is noteworthy due to the fact that the *dodeca*methoxo-cluster is not formed.

As will be shown further down, the cyclic voltammogram of **1** reveals several reversible redox transitions, bringing about the synthetic endeavor of chemically producing and isolating redox derivatives of the neutral cluster species. This was pursued following the reduction and oxidation procedures which had successfully been applied to the *dodeca*methoxo-cluster series.[9,10]

Accordingly, reacting **1** with a mixture of chlorine and antimony pentachloride in dichloromethane leads to the formation of the single oxidation derivative in $[V_6O_8(OCH_3)_{11}][SbCl_6]$ (**2**). The oxidative strength of the $Cl_2/SbCl_5$ mixture, however, is insufficient for further oxidation to the dicationic cluster $[V_6O_8(OCH_3)_{12}]^{2+}$. The dicationic species should, however, be accessible through electrosynthesis.

X-Ray Structure Analysis. $[V_6O_8(OCH_3)_{11}]$ (**1**) crystallizes in the monoclinic space group $P2_1/n$ and contains two formula units in the unit cell. The asymmetric unit thus comprises half of a formula unit, that is, three crystallographically independent vanadium atoms. The crystallographic data for **1** is found in Table 1 and the crystal structure of the asymmetric unit is displayed in Figure 2.

Completing the structure of the molecule in the crystal by inversion of the asymmetric unit in O(123), however, falsely

(25) Gritzner, G.; Kuta, J. *Pure Appl. Chem.* **1984**, *56*, 461.

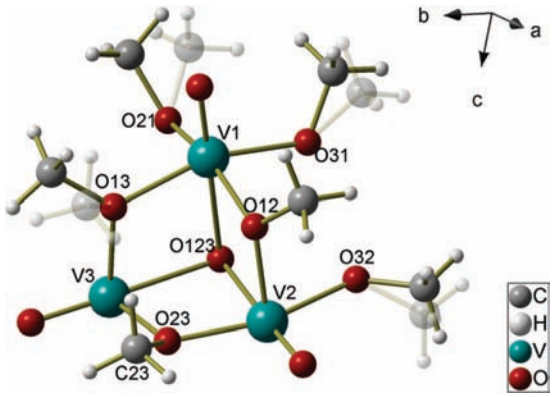

Figure 2. Asymmetric unit of the crystal structure of **1**. Conformational disorder of the methyl groups is represented by a solid and a transparent methyl ligand respectively bound to the same oxygen atom.

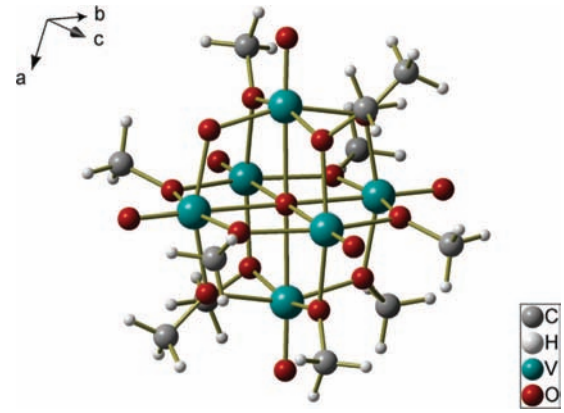

Figure 3. X-ray structural result for the molecular structure of $[V_6O_8(OCH_3)_{11}]$ (**1**).

yields the *dodeca*methoxo-cluster $[V_6O_7(OCH_3)_{12}]$. Due to the high quality of this structural solution (residual values, thermal ellipsoids, etc.), and with no physical or chemical indication at the time which were to contradict this result, the initial X-ray crystal structure solution of **1** offered the erroneous result that this compound was in fact the neutral *dodeca*methoxo-cluster.[9]

Electrochemical investigations provided the first physical evidence of a discrepancy and prompted a reevaluation of the diffraction data. In particular, upon scrutinizing the structure solution of **1** (Figure 2), a closer look at the bond lengths reveals a mean value of 1.899 Å for the V−O(23) distances, which markedly deviates from the average value of 1.975 Å obtained for the remaining V−O_b distances. In addition to this, an anomalously large value of 1.529 Å is observed for the O(23)−C(23) bond length.

Accordingly, these observations suggested a possible occupational disorder of the methyl group at the C(23) position. This was confirmed when refining this position anew with an occupational factor of 0.5, upon which the original residual value R_1 dropped from 0.0402 for full occupancy, to 0.0346 for an occupancy of 50%. Setting a free variable for the occupational factor of the methyl position yielded a value of 0.49 after least-squares refinement. Thus, for O(23) and its symmetry equivalent position in the cluster molecule, only one of the two positions actually accommodates a methyl ligand. These μ-bridging sites are therefore subject to substitutional disorder between an oxo and a methoxo ligand. The correct solution of the X-ray diffraction data of **1** therefore yields the molecular structure shown in Figure 3, with the chemical formula $[V_6O_8(OCH_3)_{11}]$. Attempts to refine the crystal structure in the noncentrosymmetric space groups *Pn* and $P2_1$ were not successful.

The structure of **1** is derived from the Lindqvist structure $[M_6O_{19}]^{n-}$ by substitution of 11 of the 12 μ-bridging oxo ligands with monodentate methoxo ligands. Thus, in contrast to the *dodeca*methoxo-cluster $[V_6O_7(OCH_3)_{12}]$ for which it was mistaken, **1** comprises one μ-bridging oxo ligand. Due to this structural difference, the neutral *undeca*methoxo-cluster **1** comprises only three V^{IV} ions, as opposed to four in $[V_6O_7(OCH_3)_{12}]$. With respect to d-electron content, **1** is therefore isoelectronic to the cationic *dodeca*methoxo-cluster $[V^{IV}{}_3V^{V}{}_3O_7(OCH_3)_{12}]^+$ reported earlier.[9,10]

The possibility that the *undeca*methoxo-cluster might contain a hydroxo ligand instead of the oxo-ligand was ruled out due to the absence of a characteristically broad and intense absorption band typical for O−H stretching in the IR-spectrum of **1**. Such a band is for example found in the IR-spectrum of the well characterized related cluster compound $[V_6O_{10}(OH)(OCH_3)_8]$ at ∼3000 cm^{-1}.[26] The chemical formula $[V^{IV}{}_3V^{V}{}_3O_8(OCH_3)_{11}]$ for **1** is also consistent with the results from valence sum calculations (*vide infra*).

$[V_6O_8(OCH_3)_{11}][SbCl_6]$ (**2**) crystallizes from dichloromethane in the triclinic space group $P\bar{1}$ and contains two formula units and two solvate molecules in the unit cell. Accordingly, the asymmetric unit comprises one formula unit.

The structure of **2** contains the $[V_6O_8(OCH_3)_{11}]^+$ cation, the single oxidation product of **1** and one of the few cationic polyoxometalate derivatives known to date.[9,10] The mixed valence cluster comprises two V^{IV} and four V^{V} ions. Thus, with respect to d-electron content, it is isoelectronic to the dicationic cluster $[V^{IV}{}_2V^{V}{}_4O_7(OCH_3)_{12}]^{2+}$ of the *dodeca*methoxo-cluster series.

As opposed to the crystal structure of $[V_6O_8(OCH_3)_{11}]$ (**1**), the cluster cation in the crystal structure of **2** displays a distinct variation of the interatomic vanadium distances due to the μ-bridging oxo ligand. Thus, the vanadium atoms which flank the μ-oxo moiety display a noticeably shorter mean interatomic distance of 3.06 Å compared to the average value of 3.23 Å for the remaining V−V distances.

Valence Sum Calculations. The primary value of the bond valence theory lies in the possibility of quantitatively predicting bond lengths from a given bond valence. As a result of this, the method can be used to test the reliability of a determined structure, to locate likely sites for atoms in substitutionally disordered materials as well as to locate weakly scattering atoms. Applied to the mixed valence compounds presented here, the bond valence method[27] is of particular interest for establishing the vanadium atoms' valence in the compounds' crystal structures, that is, for determining the respective arrangement of V^{IV} and V^{V} ions in the hexavanadate core. In this respect, results indicating valence averaging formally suggest a substitutional disorder of the V^{IV} and V^{V} ions at those positions, reflecting d-electron delocalization between these sites.

The valence sum calculations presented here were performed on crystal structure data obtained at 173 K. The bond valence parameters for vanadium bound to oxygen, as well as the "universal" constant *b* were taken from *Brese* and *O'Keeffe*.[28]

(26) Daniel, C. *Doctoral Thesis*, Freie Universität Berlin, Germany, 2005; see also the Supporting Information.
(27) Rohrer, G. S. *Structure and Bonding in Crystalline Materials*; Cambridge University Press: Cambridge, 2001; pp 440−449.
(28) Brese, N. E.; O'Keeffe, M. *Acta Crystallogr.* **1991**, *B47*, 192–197.

Table 2. Valence Sums for the Crystallographically Independent Vanadium Atoms in **1** Obtained from Crystal Structure Data Collected at 173 K

compound		bond-valence sums V(1)	V(2)	V(3)
$[V^{IV}_3V^{V}_3O_8(OCH_3)_{11}]$ (**1**)	V^{IV}	**4.11**	4.51	4.67
	V^{V}	4.33	4.74	**4.92**

Table 3. Valence Sums for the Crystallographically Independent Vanadium Atoms in **2** · CH_2Cl_2 Obtained from X-Ray Structural Data Collected at 173 K

compound		bond-valence sums V(1)	V(2)	V(3)	V(4)	V(5)	V(6)
$[V_6O_8(OCH_3)_{11}][SbCl_6]$ (**2**) · CH_2Cl_2	V^{IV}	4.74	4.73	**4.24**	4.75	**4.24**	4.81
	V^{V}	**4.99**	**4.98**	4.46	**5.00**	4.46	**5.06**

Calculations were performed on the crystographically independent vanadium atoms for the valences +IV and +V respectively.

Valence sum calculations conducted on the crystallographically independent vanadium atoms in $[V^{IV}_3V^{V}_3O_8(OCH_3)_{11}]$ (**1**) are listed in Table 2. They reveal localized valences (V^{IV} for V(1) and V^{V} for V(3)) for two of the three vanadium positions in the asymmetric unit (Figure 2), that is, for four sites in the cluster molecule. The result for the third vanadium position V(2) is necessarily a mixed valence, since the crystallographic inversion center located at the position of the central oxygen atom O(123) only allows an even number of vanadium (+IV) valences to adopt a geometry with localized valences.

Valence sum calculations conducted on the crystallographically independent vanadium atoms in $[V^{IV}_2V^{V}_4O_8(OCH_3)_{11}][SbCl_6]$ (**2**) · CH_2Cl_2 presented in Table 3 indicate a localization of the valences, the V^{IV} valences in V(3) and V(4) adopting a trans arrangement with respect to the central oxygen atom in the crystal structure. As can be expected for electrostatic reasons, the dinegative μ-bridging oxo ligand is flanked by V^{V}. This results from the higher electrophilicity of the vanadium ions in their highest oxidation state, in combination with the increased charge density of the dianionic μ-bridging oxo ligand compared to its mononegative methoxo homologues. This also brings about a distinctly shorter V−V distance for these positions, leading to the distortion of the vanadium centers' nearly octahedral arrangement in the structure discussed in the foregoing. There is, however, no indication of an analogous displacement of the vanadium nuclei in the crystal structure of **1**.

Electrochemistry. The methoxo-polyoxovanadium clusters presented here were investigated by cyclic voltammetry. Linear sweep or cyclic voltammetries are employed as simple, flexible routine techniques and, in particular, as a sophisticated means of solving chemical and mechanistic problems.[29,30] Thus, determination of reactive intermediates and the analysis of reaction kinetics is a major application of cyclic voltammetry, together with the characterization of the thermodynamics of redox systems.

The choice of solvents and supporting electrolytes for cyclovoltammetric studies depends on the specific application and other factors such as the stability or the solubility of the substrate. For the present investigations, the use of acetonitrile proved advantageous due to its good solvation properties and, in particular, to its high resistance toward electrochemical decomposition. Both qualities are essential for the investigation of the present cluster series which are redox active over a wide potential range.

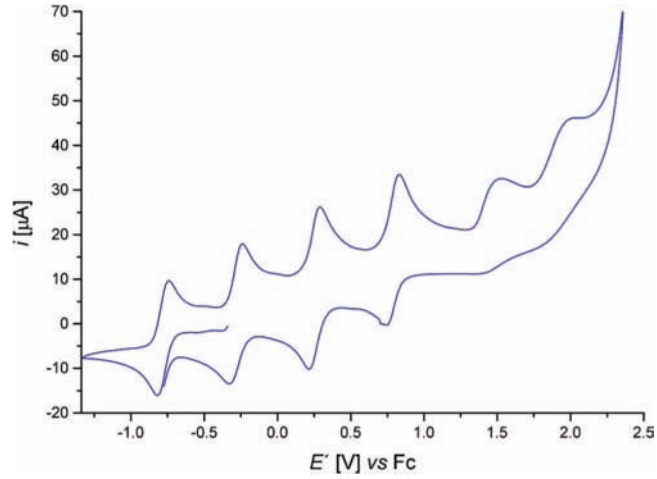

Figure 4. Cyclic voltammogram of $[V^{IV}_5V^{V}_1O_7(OCH_3)_{12}]^-$ (tetrabutylammonium salt) measured in acetonitrile and referenced against the ferrocene/ferrocenium couple (scan rate: 200 $mV \cdot s^{-1}$).

Previous results[10] from cyclovoltammetric experiments obtained for the $[V_6O_7(OCH_3)_{12}]$ cluster series in dichloromethane have therefore presently been extended to the entire range of electrochemical activity, allowing the detection of all feasible electrochemical transitions. For this purpose, the mononegative cluster anion $[V_6O_7(OCH_3)_{12}]^-$ as its tetrabutylammonium salt was employed, giving the best results with respect to the criteria of reversibility, and hence providing the greatest accuracy in determining the redox potentials. Thanks to its high solubility, the use of tetrabutylammonium as the counterion helps prevent undesirable effects in solution such as, for example, ion pairing.

The cyclic voltammogram of $[V_6O_7(OCH_3)_{12}]^-$ is shown in Figure 4. The zero current potential leg located on the inside of the cyclic voltammogram indicates the starting point of the experiment at which the solution only contains the mononegative $[V^{IV}_5V^{V}O_7(OCH_3)_{12}]^-$ cluster species. Whereas only four redox transitions could be detected in dichloromethane,[10] the electrochemical experiment performed in acetonitrile allows the detection of six single electron transfers. Accordingly, the entire range of electrochemical transformation is measured, from full reduction to the isovalent vanadium(+IV) cluster species $[V^{IV}_6O_7(OCH_3)_{12}]^{2-}$, to complete oxidation in the vanadium(+V) cluster $[V^{V}_6O_7(OCH_3)_{12}]^{4+}$, thereby encompassing *seven* isostructural hexavanadium compounds with varying V^{IV} content.

In the cyclic voltammogram of $[V_6O_7(OCH_3)_{12}]^-$, the last two electrochemical transformations are partly irreversible, indicating subsequent chemical reaction of the oxidized species. On the other hand, the sharp increase in the anodic current at the positive turning potential signalizes the oxidation of acetonitrile and, accordingly, the limit of the cyclovoltammetric experiment for this solvent.

The cyclic voltammogram of $[V_6O_8(OCH_3)_{11}]$ (**1**) is shown in Figure 5, the zero current potential leg located on the inside of the cyclic voltammogram again indicating the starting point of the experiment at which the solution exclusively contains **1**. As opposed to the *dodeca*methoxo-cluster series, however, the cyclic voltammogram of the *undeca*methoxo-cluster species displays only *five* redox transitions. Thus, a sequence of six hexavanadium clusters with varying V^{IV} content is detected in

(29) Heinze, J. *Angew. Chem., Int. Ed. Engl.* **1984**, *23*, 831–847.
(30) Speiser, B. In *Encyclopedia of Electrochemistry*; Bard, A. J., Stratmann, M., Eds.; Wiley-VCH: Weinheim, 2003; Vol. 3, pp 81−104.

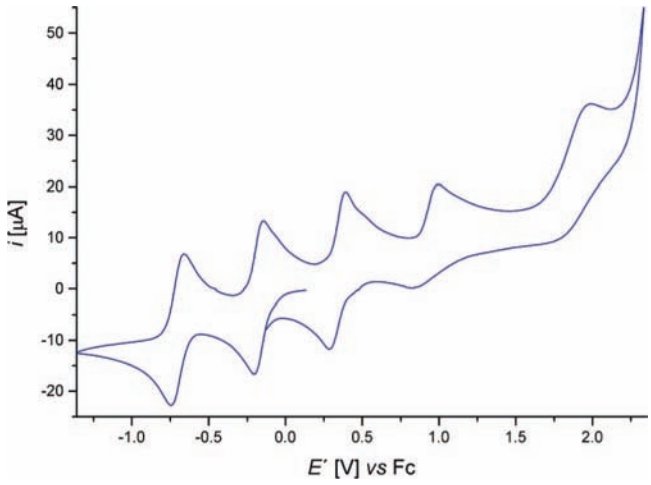

Figure 5. Cyclic voltammogram of $[V^{IV}{}_3V^{V}{}_3O_8(OCH_3)_{11}]$ (**1**) measured in acetonitrile and referenced against the ferrocene/ferrocenium couple (scan rate: 200 mV·s^{-1}).

the electrochemical experiment, ranging from the methoxo-polyoxovanadate dianion $[V^{IV}{}_5V^{V}{}_1O_8(OCH_3)_{11}]^{2-}$ up to the completely oxidized $[V^{V}{}_6O_8(OCH_3)_{11}]^{3+}$ cluster. Interestingly, a reduction step to the fully reduced vanadium(+IV) cluster species is not detected in the cyclic voltammogram of the *undeca*methoxo-cluster series.

As in the cyclic voltammogram of the *dodeca*methoxo-cluster series, the last two oxidation steps in the cyclovoltammogram of **1** are partly irreversible. When using a less positive turning potential ($\leq$+1.5 V), however, the second to the last redox transition becomes fully reversible, with a redox potential of + 0.94 V vs Fc.

The redox potentials $E^{0\prime}$ vs Fc for both cluster series are listed in Table 4. The values for the redox couples involving the highly charged cluster species $[V_6O_7(OCH_3)_{12}]^{3+/4+}$ and $[V_6O_8(OCH_3)_{11}]^{3+}$ bear a greater amount of inaccuracy due to the fact that they are respectively formed in a partly irreversible electrochemical process. Compared with known oxidizing agents,[31] these highly oxidized cationic cluster-species exhibit unusually high redox potentials, opening the prospect of using them as potent oxidizing agents in chemical synthesis.

As can be taken from Table 4, the electrochemical potential separations $\Delta E^{0\prime}$ between successive one-electron redox events in the cyclic voltammograms of $[V_6O_7(OCH_3)_{12}]^{-}$ and **1** are considerable. Due to these large separations ($\Delta E^{0\prime} > 150$ mV), the cyclic voltammograms consist of a sequence of well resolved one-electron transfer waves.

The redox process as a whole, however, is more complicated than appears at first sight. In particular, at the same time as the heterogeneous electron-transfer at the electrode interface takes place, fast homogeneous electron-transfer reactions also occur, which, in multielectron transfer systems, lead to disproportionation or comproportionation.[29] Hence, a succession of two single electron transfers (I) can in principle be treated as a disproportionation mechanism (II):

$$\mathrm{Red(2)} \underset{+e^-}{\overset{-e^-}{\rightleftharpoons}} \mathrm{Red(1)} \underset{+e^-}{\overset{-e^-}{\rightleftharpoons}} \mathrm{Ox} \qquad \text{(I)}$$

$$2\mathrm{Red(1)} \rightleftarrows \mathrm{Ox} + \mathrm{Red(2)} \qquad \text{(II)}$$

Since the equilibrium position for the disproportionation of Red(1) is usually reached within the time-scale of voltammetric measurements, the disproportionation constant $K = [\mathrm{Ox}] \cdot [\mathrm{Red(2)}]/[\mathrm{Red(1)}]^2$ can be derived from the difference between the standard potentials using $-RT \cdot \ln K = nF\,(E_1^{0\prime} - E_2^{0\prime})$. In this equation, $E_1^{0\prime}$ and $E_2^{0\prime}$ are the electrochemical potentials for the reduction and oxidation of Red(1), respectively.

Accordingly, the magnitude of $\Delta E^{0\prime}$ for two successive redox transformations reflects the thermodynamic stability of the electrochemical species involved in both redox processes, in this case Red(1). This consideration will prove of great value for discussing factors influencing the magnititude of $\Delta E^{0\prime}$ since they are inherently linked to the characteristics of the chemical species which is defined by the potential gap.

In view of the above, the large potential separations displayed in the cyclic voltammograms of both the *dodeca*methoxo- and *undeca*methoxo-cluster series corresponds to a high thermodynamic stability of the respective mixed valence cluster species with regard to their disproportionation. As shown in Table 5, their *comproportionation* constants $K_c = K^{-1}$ generally range from 10^8 to 10^{10}. For the d^1-cluster $[V^{IV}{}_1V^{V}{}_5O_8(OCH_3)_{12}]^{2+}$, however, K_c nearly reaches 10^{16}. This exceptional comproportionation constant constitutes a surprising discrepancy which in the following will prove to be essential for the inquiry on the influence exerted by a μ-bridging oxo ligand in these cluster systems.

In Figure 6, both the cyclic voltammograms of the *dodeca*- and the *undeca*methoxo-cluster series are shown for comparison. The redox potentials for the respective transitions are indicated by a solid line. To either side of the electrochemical transformation steps, the respective reduced and oxidized cluster species involved in the single electron transfer are displayed. Corresponding redox transitions in the cluster series with respect to the number of paramagnetic vanadium(+IV) ions in the hexanuclear core are indicated by a dotted line.

Upon comparing the cyclic voltammograms, one notices that the most positive redox transition for both series occurs at approximately the same potential ($\sim$ +1.9 V). This is not surprising since the minor structural- and charge differences between the corresponding clusters would not be expected to induce a considerable electrochemical potential shift. The following redox potentials, however, regularly show a large discrepancy, the respective electrochemical transformations occurring at far lower potentials for the *undeca*methoxo-cluster. As a result of this, an exceptionally large potential gap $\Delta E^{0\prime}$ of almost 1 V is observed between the two most positive redox potentials in the cyclic voltammogram of $[V_6O_8(OCH_3)_{11}]$ (**1**). Further transitions, however, are separated by relatively constant potential intervals of around 550 mV, in good correspondence to the $\Delta E^{0\prime}$ values found throughout for the *dodeca*methoxo-cluster series (Table 6).

In view of this unexpected feature in the cyclic voltammogram of **1**, it should be reminded that the potential separations $\Delta E^{0\prime}$ are the result of *electronic interactions* between the redox-active sites. Among the phenomena underlying the separation, the size of the potential gap is primarily a function of electronic delocalization, superexchange- and electrostatic interactions.[32]

(31) Connelly, N. G.; Geiger, W. E. *Chem. Rev.* **1996**, *96*, 877–910.

(32) (a) Gagné, R. R.; Spiro, C. L. *J. Am. Chem. Soc.* **1980**, *102*, 1443–1444. (b) Crutchley, R. J. In *Comprehensive Coordination Chemistry II*; McCleverty, J. A., Meyer, T. J., Eds.; Elsevier: Oxford, 2004; Vol. 2, pp 235−244.

Table 4. Redox Potentials Obtained from the Cyclic Voltammograms of $[V_6O_7(OCH_3)_{12}]^-$ (Tetrabutylammonium salt) and **1**[a]

redox process	$E^{0\prime}$ vs Fc in CH_3CN	
	$[V_6O_7(OCH_3)_{12}]^-$ ($n = 0$)	$[V_6O_8(OCH_3)_{11}]$ **1** ($n = 1$)
$[V^{IV}{}_1V^{V}{}_5O_{7+n}(OCH_3)_{12-n}]^{(3-n)+} \rightleftharpoons [V^{V}{}_6O_{7+n}(OCH_3)_{12-n}]^{(4-n)+} + e^-$	≈ +1.9 V	≈ +1.9 V
$[V^{IV}{}_2V^{V}{}_4O_{7+n}(OCH_3)_{12-n}]^{(2-n)+} \rightleftharpoons [V^{IV}{}_1V^{V}{}_5O_{7+n}(OCH_3)_{12-n}]^{(3-n)+} + e^-$	≈ +1.4 V	+0.94 V
$[V^{IV}{}_3V^{V}{}_3O_{7+n}(OCH_3)_{12-n}]^{(1-n)+} \rightleftharpoons [V^{IV}{}_2V^{V}{}_4O_{7+n}(OCH_3)_{12-n}]^{(2-n)+} + e^-$	+0.79 V	+0.36 V
$[V^{IV}{}_4V^{V}{}_2O_{7+n}(OCH_3)_{12-n}]^{n-} \rightleftharpoons [V^{IV}{}_3V^{V}{}_3O_{7+n}(OCH_3)_{12-n}]^{(1-n)+} + e^-$	+0.25 V	−0.19 V
$[V^{IV}{}_5V^{V}{}_1O_{7+n}(OCH_3)_{12-n}]^{(1+n)-} \rightleftharpoons [V^{IV}{}_4V^{V}{}_2O_{7+n}(OCH_3)_{12-n}]^{n-} + e^-$	−0.28 V	−0.73 V
$[V^{IV}{}_6O_{7+n}(OCH_3)_{12-n}]^{(2+n)-} \rightleftharpoons [V^{IV}{}_5V^{V}{}_1O_{7+n}(OCH_3)_{12-n}]^{(1+n)-} + e^-$	−0.78 V	−

[a] $c = 10^{-3}$ M; sweep rate = 200 mV/s.

Table 5. Comproportionation Constants K_c (298 K) of the Mixed Valence Clusters of the *Dodeca*methoxo- and *Undeca*methoxo-Cluster Series in Acetonitrile[a]

mixed valence cluster	K_c (298 K) in CH_3CN	
	$[V_6O_7(OCH_3)_{12}]^-$ ($n = 0$)	$[V_6O_8(OCH_3)_{11}]$ **1** ($n = 1$)
$[V^{IV}{}_1V^{V}{}_5O_{7+n}(OCH_3)_{12-n}]^{(3-n)+}$	≈1.3×10^8	≈7.6×10^{15}
$[V^{IV}{}_2V^{V}{}_4O_{7+n}(OCH_3)_{12-n}]^{(2-n)+}$	≈1.4×10^{10}	6.7×10^9
$[V^{IV}{}_3V^{V}{}_3O_{7+n}(OCH_3)_{12-n}]^{(1-n)+}$	1.1×10^9	2.1×10^9
$[V^{IV}{}_4V^{V}{}_2O_{7+n}(OCH_3)_{12-n}]^{n-}$	9.9×10^8	1.4×10^9
$[V^{IV}{}_5V^{V}{}_1O_{7+n}(OCH_3)_{12-n}]^{(1+n)-}$	3.6×10^8	−

[a] $RT \ln K_c = n F (E^{0\prime}{}_1 - E^{0\prime}{}_2)$.

As has already been demonstrated for the *dodeca*methoxo- and -ethoxo-cluster series,[10] however, the magnitude of $\Delta E^{0\prime}$ for the mixed valence *undeca*methoxo-clusters is mainly attributed to the extensive delocalization of the d-electrons.

The similarity of all but one of the $\Delta E^{0\prime}$ values for the present cluster series shown in Table 6 indicates that the contribution arising from electronic delocalization in the mixed valence species to the size of the potential gap should be comparable for all species. Accordingly, an equivalent contribution from delocalization can reasonably be expected for the *undeca*methoxo-cluster $[V^{IV}{}_1V^{V}{}_5O_8(OCH_3)_{11}]^{2+}$, which is the mixed valence species directly associated to the exceptionally high $\Delta E^{0\prime}$ value in the cyclic voltammogram of **1** (Figure 6). The same also applies for the smaller contribution to the respective potential gaps arising from electrostatic interactions in the different mixed valence cluster species.

We therefore come to the conclusion that the increased $\Delta E^{0\prime}$ value in the cyclic voltammogram of **1** must be the result of an exceptional contribution arising from superexchange interactions. Although there are no such interactions in the $[V^{IV}{}_1V^{V}{}_5O_8(OCH_3)_{11}]^{2+}$ cluster itself, since it has only a single paramagnetic electron, spin−spin interactions are possible in the reduced species $[V^{IV}{}_2V^{V}{}_4O_8(OCH_3)_{11}]^+$, the stability of which influences the *lower redox potential* (i.e., $E^{0\prime}$ for the $[V_6O_8(OCH_3)_{11}]^+ \rightleftharpoons [V_6O_8(OCH_3)_{11}]^{2+} + e^-$ conversion) of the $\Delta E^{0\prime}$ gap in question. In particular, superexchange interactions between paramagnetic d-electrons in the reduced species may either lead to a stabilization or a destabilization of the $[V^{IV}{}_2V^{V}{}_4O_8(OCH_3)_{11}]^+$ cluster cation.

Thus, the stabilization of this species through superexchange would be expected to result in a potential shift toward a more positive $E^{0\prime}$-value for its oxidation, thus reducing the magnitude of the potential gap $\Delta E^{0\prime}$ for the $[V^{IV}{}_1V^{V}{}_5O_8(OCH_3)_{11}]^{2+}$ cluster species. As opposed to this, *destabilization* through superexchange interactions would lead to a shift toward a more negative potential for the reduction of $[V^{IV}{}_1V^{V}{}_5O_8(OCH_3)_{11}]^{2+}$, thus *increasing* $\Delta E^{0\prime}$. This corresponds to what is actually observed in the cyclic voltammogram of the *undeca*methoxo-cluster series, since the potential gap is considerably larger than the usual magnitude of separation for successive redox potentials observed in both the *undeca*methoxo- and *dodeca*methoxo-cluster series (Table 6).

We therefore conclude from this observation, that the negative potential barrier for the introduction of a second electron into the hexanuclear core of the *undeca*methoxo-cluster species is increased by a destabilizing superexchange interaction which is effective in the reduced species $[V^{IV}{}_2V^{V}{}_4O_8(OCH_3)_{11}]^+$. Support for adopting this hypothesis involves the fact that the strong deviation in otherwise very similar $\Delta E^{0\prime}$ values for the *undeca*methoxo-cluster series occurs at the redox step involving the addition or removal of a *second* d-electron, that is, *the formation of an electronic condition in which magnetic interaction between unpaired electrons is first made possible*.

In particular, considering the fact that the presence of a bridging μ-oxo ligand in the *undeca*methoxo-clusters is the only chemical difference between the *dodeca*methoxo- and *undeca*methoxo-cluster series, we tentatively attribute the repeated discrepancy of approximately 450 mV between corresponding redox potentials $E^{0\prime}$ of the cluster series involving cluster species in which superexchange interactions are effective (i.e., containing two or more d-electrons: see Table 4 and Figure 6) to the presence of strong magnetic exchange interactions in the *undeca*methoxo-cluster species which are mediated by the μ-bridging oxo ligand.

Although no magnetic data is currently available for the *undeca*methoxo-cluster series in further support of this conclusion, it is generally observed that μ-bridging oxo ligands mediate strong to very strong *antiferromagnetic exchange* in polyoxovanadates(IV) compared to μ-bridging alkoxo ligands.[33,34] We are presently not aware of an account of the strength of antiferromagnetic interaction for a single bent oxo ligand in a V^{IV} complex, yet a linear μ-oxo bridged divanadate(+IV) complex has been reported which displays very strong antiferromagnetic coupling, the substance being diamagnetic even at room temperature.[35] In any case, the importance of the potential shift observed in the cyclic voltammogram of the *undeca*methoxo-cluster series clearly indicates that a strong effect is at work which is linked to the properties of the μ-bridging oxo-ligand.

Magnetism. In the following, we present results from magnetic measurements conducted on the *dodeca*methoxo-cluster compounds $N(n\text{-}C_4H_9)_4[V_6O_7(OCH_3)_{12}]$ and $[N(n\text{-}C_4H_9)_4]_2[V_6O_7(OCH_3)_{12}]$, which both display net antiferromagnetic exchange interactions between the V^{IV} centers.

The inverse Curie plot for $N(n\text{-}C_4H_9)_4[V^{IV}{}_5V^{V}O_7(OCH_3)_{12}]$ is displayed in Figure 7. Due to the curvature of the inverse

(33) Karet, G. B.; Sun, Z.; Heinrich, D. D.; McCusker, J. K.; Folting, K.; Streib, W. E.; Huffman, J. C.; Hendrickson, D. N.; Christou, G. *Inorg. Chem.* **1996**, *35*, 6450–6460.
(34) Müller, A.; Peters, F.; Pope, M. T.; Gatteschi, D. *Chem. Rev.* **1998**, *1*, 239–272.
(35) Toftlund, H.; Larsen, S.; Murray, K. S. *Inorg. Chem.* **1991**, *30*, 3964–3967.

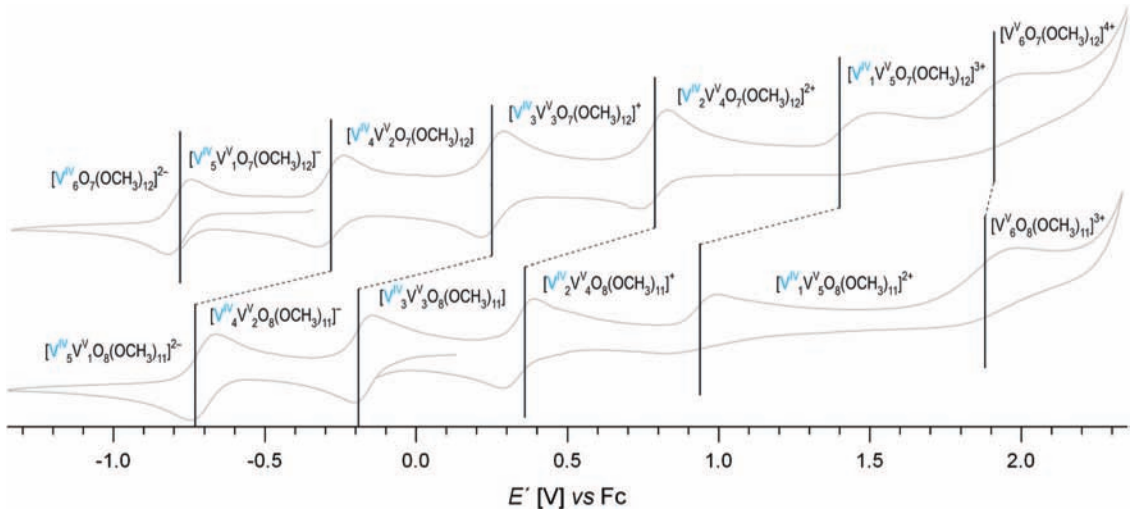

Figure 6. Electrochemical behavior of the *dodeca*methoxo- (upper cyclic voltammogram) and *undeca*methoxo-cluster species (lower cyclic voltammogram).

Table 6. Redox Potential Separations $\Delta E^{0\prime}$ for the $[V^{IV}_nV^{V}_{6-n}O_7(OCH_3)_{12}]^{(4-n)}$ ($n = 0-6$) and $[V^{IV}_nV^{V}_{6-n}O_8(OCH_3)_{11}]^{(3-n)}$ ($n = 0-5$) Cluster Series Respectively Obtained from the Cyclic Voltammograms of $[V_6O_7(OCH_3)_{12}]$ and $[V_6O_8(OCH_3)_{11}]$ (**1**) in Acetonitrile

	$\Delta E^{0\prime}$ in CH_3CN	
Red_j / Ox_i ↔ Red_j / Ox_j	$[V_6O_7(OCH_3)_{12}]$	$[V_6O_8(OCH_3)_{11}]$ (**1**)
$\{V^{IV}_2V^{V}_4\}/\{V^{IV}_1V^{V}_5\}$ ↔ $\{V^{IV}_1V^{V}_5\}/\{V^{V}_6\}$	~500 mV	~**950** mV
$\{V^{IV}_3V^{V}_3\}/\{V^{IV}_2V^{V}_4\}$ ↔ $\{V^{IV}_2V^{V}_4\}/\{V^{IV}_1V^{V}_5\}$	~600 mV	580 mV
$\{V^{IV}_4V^{V}_2\}/\{V^{IV}_3V^{V}_3\}$ ↔ $\{V^{IV}_3V^{V}_3\}/\{V^{IV}_2V^{V}_4\}$	530 mV	550 mV
$\{V^{IV}_5V^{V}_1\}/\{V^{IV}_4V^{V}_2\}$ ↔ $\{V^{IV}_4V^{V}_2\}/\{V^{IV}_3V^{V}_3\}$	530 mV	540 mV
$\{V^{IV}_6\}/\{V^{IV}_5V^{V}_1\}$ ↔ $\{V^{IV}_5V^{V}_1\}/\{V^{IV}_4V^{V}_2\}$	510 mV	–

magnetic susceptibility data at low temperatures, higher temperature values of χ^{-1} were used for determining the Weiss-constant θ. Thus, extrapolation of the inverse molar susceptibility χ^{-1} in this temperature region (red line) yields $\theta = -53$ K.

The effective magnetic moment per V^{IV} ion as a function of the temperature is displayed in Figure 8. The antiferromagnetic exchange interactions between the paramagnetic electrons afford $\mu_{eff} = 1.48\ \mu_B$ per V^{IV} ion at 300 K (the spin-only value for vanadium(+IV) is 1.73 μ_B for $g = 2.00$).

The antiferromagnetic exchange interactions increase upon addition of a further electron in the isovalent V^{IV} species $[N(n\text{-}C_4H_9)_4]_2[V^{IV}_6O_7(OCH_3)_{12}]$ (Figure 9), for which a Weiss-constant of $\theta = -147$ K (red line) is obtained. The temperature dependency of the effective magnetic moment per V^{IV} ion is shown in Figure 10, displaying an effective magnetic moment $\mu_{eff} = 1.21\ \mu_B$ per V^{IV} ion at 300 K.

With respect to the Lindqvist structure (Figure 1), little attention has yet been paid to the fact that when paramagnetic centers therein are antiferromagnetically coupled, this inherently results in a spin frustrated system.[36] Figure 11 illustrates the simplest case of spin frustration comprising a system of three antiferromagnetically coupled spins which form a triangle. As can be easily seen, it is impossible in such an odd-membered ring to simultaneously satisfy the condition of antiparallel alignment between all neighboring spins: when two spins are antiferromagnetically coupled, the third spin cannot align in an antiparallel fashion to both spins, a situation which we have depicted using a circular spin-symbol. As a result of this, the system is said to experience spin-frustration, also referred to as (geometric) magnetic-frustration.

In the Lindqvist structure, the metal sites which can accommodate unpaired electrons ideally form a regular octahedron. Since this geometrical figure is composed of eight equilateral triangles, the aforementioned spin frustration may be effective on each of the octahedron's faces (Figure 12).

The spin arrangements shown in Figures 11 and 12 are, however, only meant to *illustrate* spin frustration for these geometries in antiferromagnetically coupled systems. The depicted alignments are *not* representative of the actual situation in such a system, particularly in an isotropic system in which no two neighboring spins can effectively adopt an antiparallel arrangement to one another.

With respect to the magnetic results obtained for $N(n\text{-}C_4H_9)_4[V^{IV}_5V^{V}O_7(OCH_3)_{12}]$ and $[N(n\text{-}C_4H_9)_4]_2[V^{IV}_6O_7(OCH_3)_{12}]$, an unusual magnetic behavior is observed at low temperatures, which we tentatively attribute to the spin frustration phenomenon. Thus, at temperatures below 100 K, the inverse Curie plots in Figures 7 and 9 respectively deviate from a linear segment reflecting antiferromagnetic exchange interactions (red line), to one characteristic of *paramagnetic* systems (green line). This applies in particular to the magnetic behavior of the isovalent vanadium(+IV) species, which exhibits a Weiss-constant (green line) of approximately 0 K in this temperature region. This magnetic response may reflect a situation in which the spins' increasing tendency to align in an antiparallel fashion with decreasing thermal motion apparently comes to a halt due to geometric spin frustration. As a result of this, the effective magnetic moment μ_{eff} ceases to decrease in this temperature region upon further cooling. This is particularly striking in the isovalent V^{IV} species, μ_{eff} adopting an almost constant value of approximately 0.80 μ_B between 10 and 30 K (Figure 10). This "paramagnetic ledge" is less pronounced for the mixed valence cluster in $N(n\text{-}C_4H_9)_4[V^{IV}_5V^{V}O_7(OCH_3)_{12}]$ (Figure 8). Below 10 K, μ_{eff} rapidly decreases as a function of the strength of the magnetic field applied to the respective samples. Down to 2 K, however, a transition to an antiparallel alignment of the paramagnetic spins is not observed in either compound.

(36) (a) Kahn, O. *Molecular Magnetism*; VCH: Weinheim, 1993; pp 241–248. (b) Kahn, O. *Chem. Phys. Lett.* **1997**, *265*, 109–114.

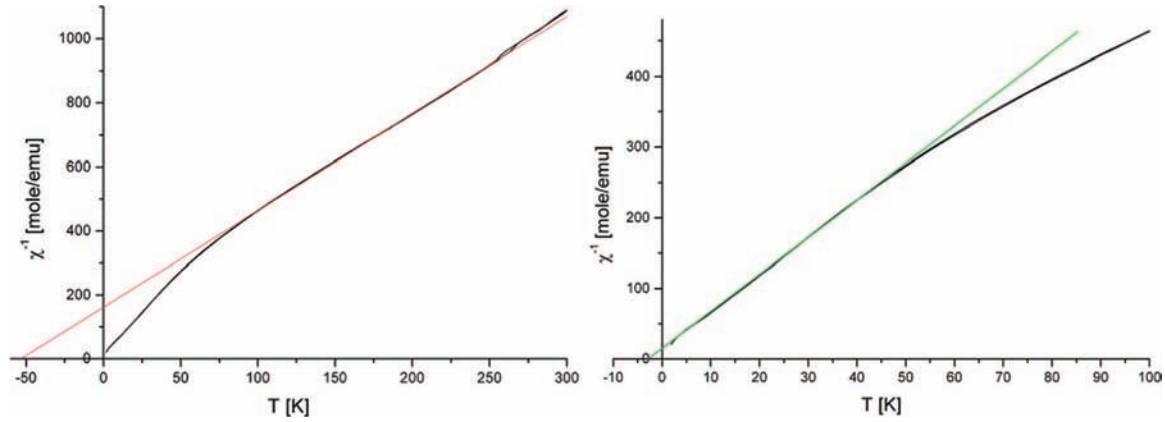

Figure 7. Inverse Curie plots for $N(n\text{-}C_4H_9)_4[V^{IV}{}_5V^{V}O_7(OCH_3)_{12}]$ ($H = 1$ T).

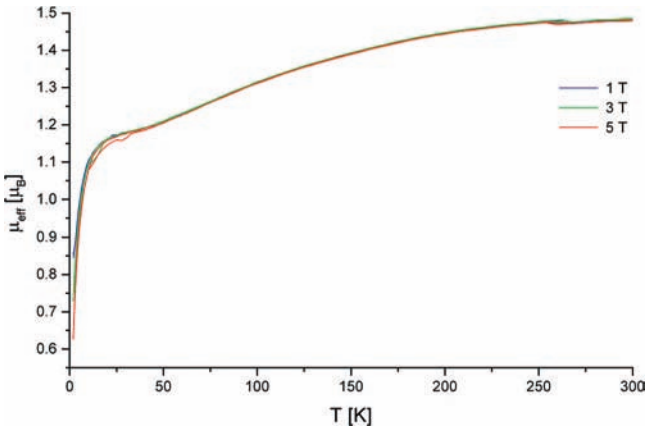

Figure 8. Temperature dependency of μ_{eff} in $N(n\text{-}C_4H_9)_4[V^{IV}{}_5V^{V}O_7(OCH_3)_{12}]$.

This particular magnetic behavior has also been observed in other spin frustrated transition metal-oxo clusters.[37,38] Interestingly, however, this behavior is not observed in Lindqvist-type polyalkoxo-hexavanadate(IV) clusters comprising trisalkoxo[8b] or a combination of trisalkoxo and hydroxo μ-bridging ligands.[8c,d] These compounds display a typically antiferromagnetic behavior in the entire temperature range, with Néel transitions to an antiferromagnetically coupled system at lower temperatures (<50 K). This behavior may result from the presence of different types of μ-bridging ligands and/or from structural factors (e.g., covalent tethering in the μ-bridging alkoxo moieties, presence of coordinating counterions) by which spin frustration might be overcome. In the case of the *dodeca*methoxo-cluster in $[N(n\text{-}C_4H_9)_4]_2[V^{IV}{}_6O_7(OCH_3)_{12}]$, however, the uniformity of the μ-bridging ligands and the presence of noncoordinating counterions assures a high structural symmetry for magnetic exchange interactions, even at low temperatures.

In the context of spin frustration, it is interesting to note that an isovalent vanadium(+IV) species has not been eluded for the *undeca*methoxo-cluster series, nor is any V^{IV} Lindqvist-type cluster known which contains μ-oxo ligands. In the present case, the cluster species with the highest reduction grade which has been detected by cyclic voltammetry in the *undeca*methoxo-cluster series is $[V^{IV}{}_5V^{V}O_8(OCH_3)_{11}]^{2-}$, which still comprises one V^{V} ion. Scanning down to highly negative potentials (−2.5 V vs Fc) in the cyclic voltammetric experiment reveals no further electron transfer.

It is therefore conceivable that a strong (antiferromagnetic) superexchange mediating ligand such as μ-oxo might amplify the degree of magnetic frustration such as to considerably destabilize the hypothetical $[V^{IV}{}_6O_8(OCH_3)_{11}]^{3-}$ cluster species. Magnetic measurements on species of the *undeca*methoxo-cluster series have yet to be conducted, however.

IR spectroscopy. As has previously been displayed for the *dodeca*methoxo- and -ethoxo-cluster series,[10] IR spectroscopy is also very useful in the analysis of the *undeca*methoxo-cluster series presented here. Thus, besides its use for fingerprinting purposes, the IR spectra equally provide reliable information on the cluster charge. Furthermore, analysis of the band shape and half-bandwidth of selected vibration modes provides insight on the extent of electronic delocalization in the mixed valence species.

In the IR spectra of the *undeca*methoxo-clusters, the 400−1200 cm^{-1} region is of particular interest, containing absorption bands due to metal−oxygen stretching vibrations which are characteristic of polyoxometalate spectra in general.[1] Thus, five characteristic absorption bands are observed in this region, the spectra showing a high resemblance to those obtained for the *dodeca*methoxo-cluster series.[10] The strongest bands are located in the 950−1100 cm^{-1} region: the O_b-CH_3 (1000−1100 cm^{-1}) and the $V-O_t$ (950−1000 cm^{-1}) stretching modes. A further absorption band located in the 550−650 cm^{-1} region is attributed to $V-O_b-V$ bending. Finally, two bands in the 400−450 cm^{-1} region are tentatively assigned to $V-O_c$ stretching.[39]

Interestingly, the only apparent difference between the IR spectra of both cluster series concerns a weak absorption band in the 650−750 cm^{-1} region found in the spectra of the *undeca*methoxo-cluster species and which is attributed to $V-O_b$-V bending involving the single μ-bridging oxo ligand. Formally speaking, the high similarity of the spectra is actually quite surprising since the *undeca*methoxo-cluster's symmetry is drastically reduced by the presence of a μ-oxo ligand compared to the highly symmetric *dodeca*methoxo-cluster. As an example, the spectra of $[V_6O_8(OCH_3)_{11}]$ (**1**) and $[V_6O_7(OCH_3)_{12}]$ are displayed for comparison in Figure 13. As

(37) (a) Libby, E.; McCusker, J. K.; Schmitt, E. A.; Folting, K.; Hendrickson, D. N.; Christou, G. *Inorg. Chem.* **1991**, *30*, 3486–3495. (b) Albela, B.; El Fallah, M. S.; Ribas, J.; Folting, K.; Christou, G.; Hendrickson, D. N. *Inorg. Chem.* **2001**, *40*, 1037–1044.

(38) Yu, S.-B.; Papaefthymiou, G. C.; Holm, R. H. *Inorg. Chem.* **1991**, *30*, 3476–3485.

(39) Rocchiccioli-Deltcheff, C.; Thouvenot, R.; Fouassier, M. *Inorg. Chem.* **1982**, *21*, 30–35.

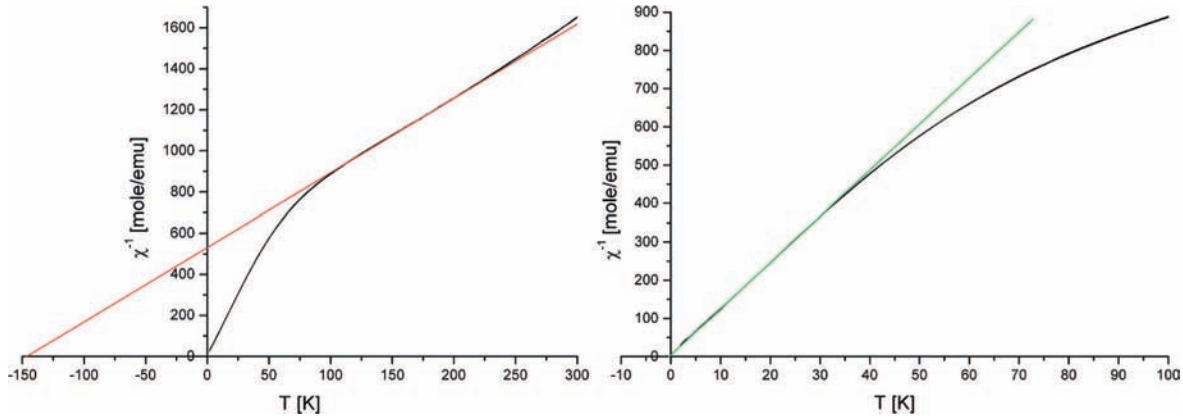

Figure 9. Inverse Curie plots for $[N(n\text{-}C_4H_9)_4]_2[V^{IV}{}_6O_7(OCH_3)_{12}]$ ($H = 1$ T).

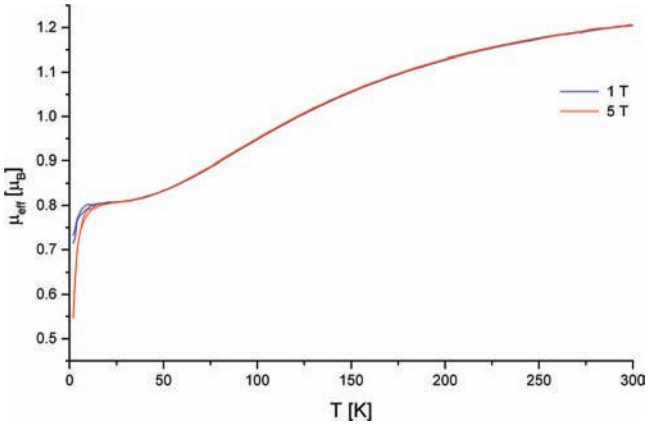

Figure 10. Temperature dependency of μ_{eff} in $[N(n\text{-}C_4H_9)_4]_2[V^{IV}{}_6O_7(OCH_3)_{12}]$.

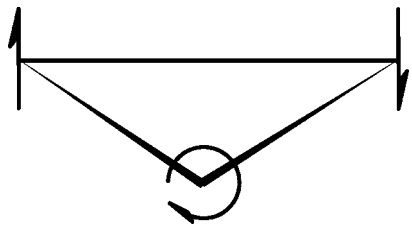

Figure 11. Spin frustration of antiferromagnetically coupled spins in a triangular geometry.

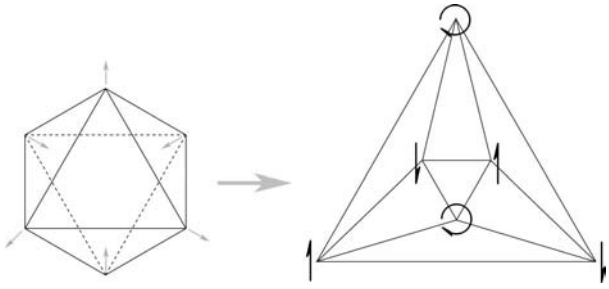

Figure 12. Two-dimensional representation (right) of spin frustration for an octahedral spin topology. The gray arrows in the octahedron (left) indicate the distortion of the representation.

can be seen, the number of absorption bands, their energies, and their intensities are essentially the same, with the exception of a weak absorption band at 715 cm^{-1} present in the spectrum of **1**. Similarly, the IR-spectrum of $[V_6O_8(OCH_3)_{11}][SbCl_6]$ (**2**)

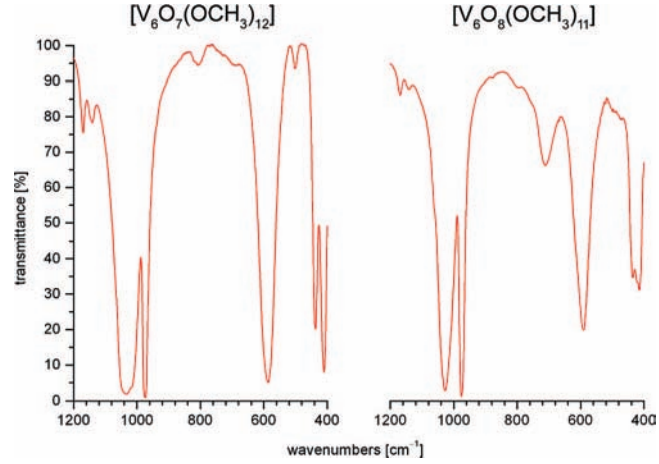

Figure 13. IR spectra of $[V_6O_7(OCH_3)_{12}]$ and $[V_6O_8(OCH_3)_{11}]$ (**1**) (KBr pellet).

is practically identical to that of $[V_6O_7(OCH_3)_{12}][SbCl_6]$, with the exception of a weak absorption at 712 cm^{-1} in the spectrum of **2**.

UV−Vis Spectroscopy. Optical spectroscopy is traditionally employed for the investigation of mixed valence compounds due to the presence of usually intense intervalence charge-transfer (IVCT) bands in the visible and ultraviolet wavelength regions of their spectra, as a result of which they are typically deeply colored in appearance.

The mixed valence *dodeca*methoxo-cluster compounds presently synthesized yield crystals which are dark green to black and which are not transparent to visible light. Their green to dark green solutions are only translucent at low concentrations. The same applies for the mixed valence *undeca*methoxo-clusters. As opposed to these mixed valence compounds, the isovalent *dodeca*methoxo-cluster compound $[N(n\text{-}C_4H_9)_4]_2[V^{IV}{}_6O_7(OCH_3)_{12}]$ yields *clear* turquoise crystals and solutions.

The UV−vis spectra of the *dodeca*methoxo-cluster series and of **1** are displayed in Figure 14. As can be seen, the absorption of the isovalent vanadium(+IV) *dodeca*methoxo-cluster species in the visible region (380−780 nm) is far less intense than its mixed-valence homologues. Being isovalent, its color is attributed to d-d transitions in the respective V^{IV} nuclei, for which absorption bands for the $d_{xy} \rightarrow d_{xz}$, d_{yz}, the $d_{xy} \rightarrow d_{x^2-y^2}$, and possibly for the $d_{xy} \rightarrow d_{z^2}$ transition can be expected based on the C_{4v} symmetry of oxovanadium(+IV) in the Lindqvist core

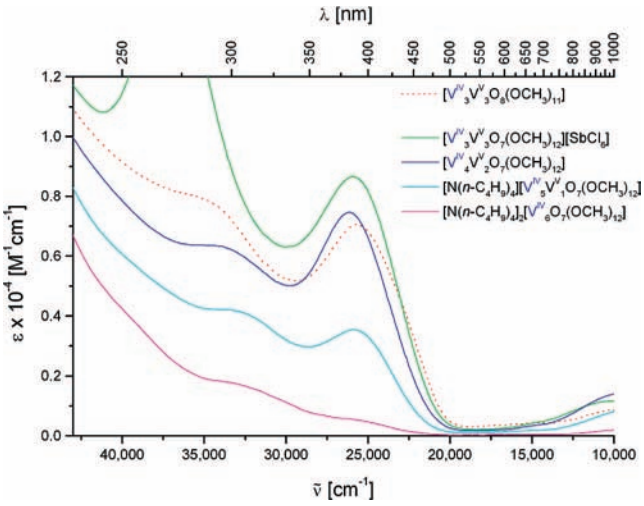

Figure 14. UV−vis spectra of the *dodeca*methoxo-cluster series (solid lines) and $[V_6O_8(OCH_3)_{11}]$ (**1**) (dotted line).

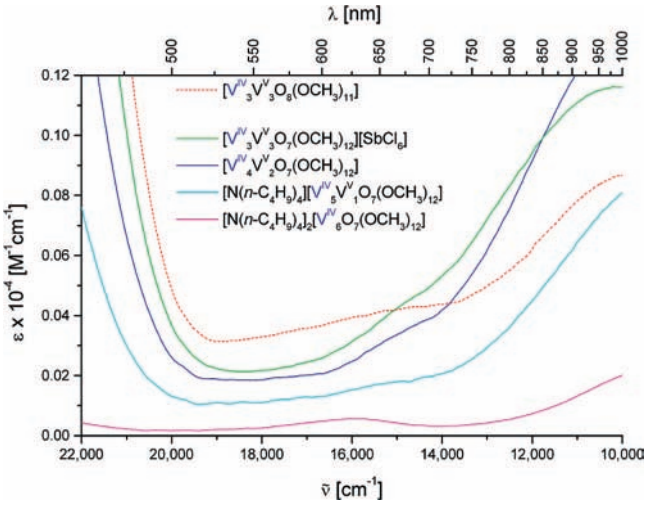

Figure 15. UV−vis spectra of the *dodeca*methoxo-cluster series (solid lines) and $[V_6O_8(OCH_3)_{11}]$ (**1**) (dotted line).

structure.[40] Accordingly, in the UV−vis spectrum of $[N(n\text{-}C_4H_9)_4]_2[V^{IV}{}_6O_7(OCH_3)_{12}]$ the absorption band with ε_{max} located in the near IR region (~1000 nm) is assigned to the $d_{xy} \rightarrow d_{xz}$, d_{yz} transition, and the shoulder with ε_{max} at 380 nm (~26 300 cm^{-1}) is tentatively attributed to the $d_{xy} \rightarrow d_z{}^2$ transition. The $d_{xy} \rightarrow d_{x^2-y^2}$ transition is only observed as a very weak absorption with ε_{max} at 630 nm (~15 900 cm^{-1}) (see Figure 15), which is consistent with the fact that the transition is forbidden for this ligand field symmetry.[8f,41]

In comparison, the UV−vis spectra of the neutral *undeca*-methoxo-cluster $[V_6O_8(OCH_3)_{11}]$ (**1**) and of the mixed valence members of the *dodeca*methoxo-cluster series all reveal two intense bands which also absorb in the visible region. The first of these has its absorption maximum ε_{max} located in the near IR region and absorbs in the red spectral range. The second has its ε_{max} located around 385 nm (~26 000 cm^{-1}) and is responsible for a strong absorption in the UV, violet, and blue spectral range.

The first of these absorptions is an IVCT band typically found in mixed valence polyoxometalates. Based on an MO diagram for the C_{4v} symmetry applicable to the respective metal sites of the Lindqvist structure,[1,42] it is attributed to d_{xy} (V^{IV}) → d_{xy} (V^V) excitation between respective V^{IV} and V^V sites.

The assignment of the second band, on the other hand, is not trivial, since both IVCT and ligand to metal charge-transfer (LMCT) bands may be expected in this region. In the absence of an electronic spectrum of a fully oxidized *dodeca*- or *undeca*methoxo-cluster species which is devoid of IVCT for comparison, it would presently reveal highly speculative to assign this band to either (or both) possibilities.

It is interesting to note, however, that in the electronic spectra of the mixed valence species, the separation between these two absorption bands roughly corresponds to the energy of the $d_{xy} \rightarrow d_{x^2-y^2}$ ligand field transition. Thus, in the UV−vis spectrum of $[V^{IV}{}_3V^V{}_3O_7(OCH_3)_{12}][SbCl_6]$, for example, ε_{max} for these bands are found at 25 900 cm^{-1} and 10 100 cm^{-1}, respectively. The difference of 15 800 cm^{-1} is in good agreement with the energy of the $d_{xy} \rightarrow d_{x^2-y^2}$ ligand field transition at 15 900 cm^{-1}, as found in the electronic spectrum of the isovalent *dodeca*-methoxo-cluster $[N(n\text{-}C_4H_9)_4]_2[V^{IV}{}_6O_7(OCH_3)_{12}]$. Accordingly, the second absorption band might at least include, if not mainly be the result of IVCT attributed to d_{xy} (V^{IV}) → $d_{x^2-y^2}$ (V^V) excitation between respective V^{IV} and V^V sites, since its energy is equal to the sum of the energies for the d_{xy} (V^{IV}) → d_{xy} (V^V) IVCT excitation and the $d_{xy} \rightarrow d_{x^2-y^2}$ ligand field transition.[43]

Finally, in the ultraviolet region (<400 nm), the absorption steadily increases toward higher wavenumbers due to oxygen to metal charge transfer. As can be seen in Figure 14, the absorption intensity for the O:→M ligand to metal charge transfer (LMCT) is correlated to the vanadium(+V) content of the respective cluster species. The strong absorption around 37 000 cm^{-1} in the UV−vis spectrum of $[V_6O_7(OCH_3)_{12}][SbCl_6]$ is attributed to $Cl{:}\rightarrow Sb^V$ LMCT.

Mixed Valency. To fully understand the chemical and physical properties of the cluster compounds presented here, it is essential to contemplate the mixed valence state common to all compounds discussed in this article, with the exception of the isovalent V^{IV} *dodeca*methoxo-cluster $[N(n\text{-}C_4H_9)_4]_2[V_6O_7(OCH_3)_{12}]$. The mixed valence phenomenon has previously been discussed in detail for compounds belonging to the *dodeca*-methoxo- and -ethoxo-cluster series,[10] results from cyclic voltammetry, X-ray structural analysis, and IR spectroscopy revealing a behavior typical of class II mixed-valence compounds according to the Robin and Day classification scheme.[14] Accordingly, depending on their physical condition and the method of measurement involved, mixed valence compounds belonging to these series display features typical of either localized or delocalized valences, as well as of valence states which can be considered as intermediate to these.

The same applies to the *undeca*methoxo-cluster compounds presented here. Thus, as shown in the foregoing, results from valence sum calculations conducted on the X-ray structural data of **1** and **2** obtained at 173 K reveal localized vanadium valences in **2**, and both localized and delocalized valences for **1**. On the other hand, the cyclic voltammogram of the *undeca*methoxo-cluster series shows large potential separations reflecting an extensive delocalization of the d-electrons in all mixed valence

(40) Garribba, E.; Micera, G.; Panzanelli, A. *Inorg. Chem.* **2003**, *42*, 3981–3987, and references cited therein.
(41) Lever, A. B. P. *Inorganic Electronic Spectroscopy*; Elsevier: Amsterdam 1984, 388.
(42) Sanchez, C.; Livage, J.; Launay, J. P.; Fournier, M.; Jeannin, Y. *J. Am. Chem. Soc.* **1982**, *104*, 3194–3202.
(43) Pope, M. T. *Heteropoly and Isopoly Oxometalates*; Springer: Berlin, 1983; p 111.

species. Furthermore, as in the case of the *dodeca*methoxo cluster series, the IR spectra of the *undeca*methoxo-clusters display a single absorption band for $V-O_t$ stretching, indicating delocalized valences even on the fast time scale of the IR experiment ($10^{-13}-10^{-14}$ s).[9,44]

In the present article, we have extended our investigation of the mixed valence phenomenon to include results from UV−vis spectrometry. In general, the investigation of IVCT bands in mixed valence compounds has received considerable attention since their analysis has been accompanied by a constant effort to interpret the experimental results with the help of theoretical models for electron transfer.[45] These have found their application in numerous binuclear compounds, for which the calculation of parameters relating to the extent of electronic coupling between metal centers of differing valency, as well as to the degree of valence delocalization has been made possible on the basis of the shape and intensity of the IVCT band.

Without proceeding to such an in-depth analysis, the UV−vis spectra of the *dodeca*methoxo-cluster series and the *undeca*-methoxo-cluster **1** do, however, reveal whether valences are localized or delocalized on the very short time-scale of the UV−vis experiment (10^{-15} s). In particular, the UV−vis spectrum of a mixed valence compound with complete electronic delocalization on this time-scale does not compare to that of a compound displaying localized valences, since absorption bands arising from excitations in the latter are not present in the electronic spectrum of the former.[46] In the present case, this concerns the $d_{xy} \rightarrow d_{xz}$, d_{yz}, the $d_{xy} \rightarrow d_{x^2-y^2}$, and the $d_{xy} \rightarrow d_{z}^2$ transitions typically found in the UV−vis spectra of oxovanadium(+IV) complexes with square pyramidal geometry,[47] and which have respectively been assigned to three absorptions found in the spectrum of the isovalent *dodeca*methoxo-cluster $[V^{IV}_6O_7(OCH_3)_{12}]^{2-}$ (*vide infra*).

Upon comparing the UV−vis spectra of the mixed valence compounds with that of the isovalent *dodeca*methoxo-cluster species (Figure 14), one immediately notices that their spectra are quite similar with respect to the energies at which absorption takes place, let aside the apparent differences in the intensity of absorption. A closer look reveals that the same applies with respect to the weak absorption band around 630 nm ($\approx$ 15,900 cm^{-1}) found in the spectra of $[N(n\text{-}C_4H_9)_4]_2[V^{IV}_6O_7(OCH_3)_{12}]$, which appears as a somewhat red-shifted shoulder in the electronic spectra of all of the mixed valence compounds (Figure 15).

For the isovalent *dodeca*methoxo-cluster, this absorption was tentatively attributed to the $d_{xy} \rightarrow d_{x^2-y^2}$ transition (*vide supra*). In a mixed valence species, however, the same (intravalent) d-d transition may only be observed if the valences are localized. Accordingly, the presence of this absorption band in the electronic spectra of the mixed valence species indicates that their valences are localized on the time scale of the UV−vis experiment.

This observation further confirms the classification of the present mixed valence species as class II mixed valence compounds according to Robin and Day[14] since, depending on the time scale of the measurement method involved, they display either localized (UV−vis spectroscopy) or delocalized valences (IR spectroscopy). In this respect, it is also interesting to note that localized valences are only noticed in experiments of which the time scale either exceeds the frequency of vibrational motion (UV−vis), or in which these vibrations are largely impaired (crystalline state and low temperatures in single-crystal X-ray diffraction), an observation which further reflects vibronic coupling in these compounds' IVCT process.[10]

Conclusion

The *undeca*methoxo-cluster $[V_6O_8(OCH_3)_{11}]$ **1** and its isostructural derivatives constitute a further series of highly interesting alkoxo-polyoxovanadium cluster compounds comprising the Lindqvist structure. Like its predecessors belonging to the *dodeca*alkoxo-cluster series, these compounds are highly redox-active and their mixed valence species show a physical behavior typical of class II mixed valence compounds.

Beyond bestowing yet a further substitution pattern of the classical polyoxometalate core structure unto this compound class, however, the narrow structural relationship of **1** to the fully methoxo-substituted Lindqvist structure $[V_6O_7(OCH_3)_{12}]$ allows a relatively straightforward comparison of their physical properties in the sense that observed differences can be directly correlated to a single structural parameter, i.e. the presence or absence of a μ-bridging oxo ligand. In this respect, we have shown that the oxo ligand's influence is particularly striking when considering the compounds' electrochemical behavior. In particular, careful interpretation of the electrochemical conversion of the highly oxidized species strongly suggests that the considerable discrepancy in the compounds' redox potentials may very well rely on a varying magnitude of spin−spin interaction between unpaired d-electrons.

A further focus of the present article concerned magnetic exchange interactions between unpaired d-electrons which, in the Lindqvist core-structure, are prone to geometric spin frustration. Thus, results from magnetic investigations conducted on the reduced species of the *dodeca*methoxo-cluster series revealed a typically antiferromagnetic behavior upon cooling, which deviates to a paramagnetic behavior at temperatures below 100 K. This unusual magnetic response resembles the one observed in other spin frustrated transition metal oxo-[37] and thio-clusters[38] and, accordingly, has tentatively been attributed to a spin frustration phenomenon effective in the high structural symmetry of the *dodeca*methoxo-cluster series.

When considering the present findings under the general aspect of polynuclear transition metal-oxo cluster chemistry, the main center of interest certainly pertains to the apparent sensitivity of the redox potentials to changes in superexchange mediated spin−spin interactions. Thus, although it is well-known that a varying degree of magnetic exchange is one of several factors which influence the size of electrochemical potential gaps,[32] the present article demonstrates that taken alone, it is actually a decisive factor for the redox behavior of the present compounds. In this context, the fact that a relatively minor structural alteration may cause such an important shift of the

(44) Demadis, K. D.; Hartshorn, C. M.; Meyer, T. J. *Chem. Rev.* **2001**, *101*, 2655–2685.

(45) (a) Hush, N. S. In *Mixed-Valence Compounds: Theory and Applications in Chemistry, Physics, Geology, and Biology*; Brown, D. B., Ed.; D. Reidel Publishing Company: Dordrecht, 1980; pp 151−188. (b) Schatz, P. N. In *Inorganic Electronic Structure and Spectroscopy*; Solomon, E. I., Lever, A. B. P., Eds.; John Wiley & Sons: New York, 1999; Vol. 2, pp 175−226, and references therein. (c) Creutz, C.; Newton, M. D.; Sutin, N. *J. Photochem. Photobiol. A: Chem.* **1994**, *82*, 47–59. (d) Hupp, J. T. In *Comprehensive Coordination Chemistry II*; McCleverty, J. A., Meyer, T. J., Eds.; Elsevier: Oxford 2004; Vol. 2, pp 709−716, and references therein.

(46) Day, P. In *Mixed-Valence Compounds: Theory and Applications in Chemistry, Physics, Geology, and Biology*; Brown, D. B., Ed.; D. Riedel Publishing Company: Dordrecht, 1980; p 16−17.

(47) (a) Ballhausen, C. J.; Gray, H. B. *Inorg. Chem.* **1962**, *1*, 111–122. (b) Bridgland, B. E.; Fowles, G. W. A.; Walton, R. A. *J. Inorg. Nucl. Chem.* **1965**, *27*, 383–389.

electrochemical potentials in the present vanadium oxide cluster species raises the exciting prospect of investigating the role this leverage-effect may play in related polynuclear transition metal oxo- and thio-clusters as they are found in a large number of metalloproteins catalyzing reactions which demand a considerable redox variability.

Hence, based on the present findings, it is postulated that, next to structural factors, already slightly varying chemical interactions (protonation, H-bonding, etc.) between such cluster moieties and their environment might induce sensible shifts in their redox-potentials mainly by means of directly influencing spin−spin interactions effective between their unpaired d-electrons. In spin frustrated systems, this effect may be additionally coupled to a varying degree of magnetic frustration. Thus, in the well defined environment of a protein, which displays a specific sequence of transformations during chemical conversion, a pronounced sensitivity of transition metal-oxo and -thio cluster redox potentials toward varying degrees of spin−spin interactions between unpaired d-electrons might be the key to an exceptional control of electron transfer in such systems.

In view of the present findings, we are convinced that the series of polymethoxo-hexa(oxovanadium) cluster compounds presented here may serve as exceptional model compounds for the investigation of magnetic exchange interactions in spin frustrated systems and, in particular, as concerns their influence on such a system's redox behavior. In this respect, the *undeca*-methoxo-cluster series $[V_6O_8(OCH_3)_{11}]^{n\pm}$ offers the exciting prospect of being able to selectively tune the degree of spin−spin interactions via its single, chemically alterable[8c] μ-oxo ligand. Furthermore, in view of their novel magnetic and electrochemical properties, these cluster compounds could prove of great interest for research and applications in materials science as well as in homogeneous and heterogeneous catalysis research. Accordingly, due to their exceptional qualities and to the numerous possibilities for their investigation, we are highly confident of these cluster series' exceptional value for current and future research purposes.

Acknowledgment. We kindly thank Mrs. Irene Brüdgam for her invaluable help in collecting the X-ray diffraction data. We equally thank Dr. Kremer of the Max Planck Institute for Solid State Research for conducting the magnetic measurements. Special thanks go to our former research students Anne-Kathrin Schmidt, Ilko Bald, Huan Cheng, Tilman Lechel, and Boris Brusilowskij for their valuable contributions to this work.

Supporting Information Available: Crystallographic data of compounds **1** and **2** (CIF files) and IR spectra of **1** and $[V_6O_{10}(OH)(OCH_3)_8]$. This material is available free of charge via the Internet at http://pubs.acs.org.

JA8073648